Shortwave absorptance in a tropical cloudy atmosphere: Reconciling calculations and observations

Kajsa Parding,[1] Laura M. Hinkelman,[2] Thomas P. Ackerman,[2] and Sally A. McFarlane[3]

Received 16 January 2011; revised 1 July 2011; accepted 8 July 2011; published 4 October 2011.

[1] The absorption of shortwave (SW) radiation by clouds is a topic surrounded by contradictory reports and controversy. Some studies have shown large discrepancies between observed SW absorption and absorption predicted by models, while others have found no significant difference. In this study, values of column SW absorptance obtained by combining collocated top-of-atmosphere (TOA) and surface observations at an island site in the tropical western Pacific are compared to radiative transfer model (RTM) output. To compensate for the field of view difference between satellite and surface instruments, the surface data are averaged over time. Scatterplots and statistical measures show that there is a significant discrepancy between models and observations with the RTMs apparently underestimating SW absorptance. The large variability of the absorptance computed from the observations, including negative values, suggests that the field of view mismatch between satellite and surface observations remains even after averaging of the surface data. This mismatch may contribute to the observation-model bias. In previous observational studies showing highly enhanced absorption compared to models, the slope of a linear fit to $d\alpha_{TOA}/dT$ (the derivative of TOA albedo with respect to transmittance) was used to quantify cloud SW absorption, while nonlinearity of $d\alpha_{TOA}/dT$ was interpreted as a sign of sampling issues. Here the models produce a steeper slope (about −0.9) than observations (−0.6 to −0.8), indicating that models predict too little cloud SW absorption. However, when the surface observations are averaged over a longer period, their slope grows steeper, and the root-mean-square difference between linear and quadratic fits to $d\alpha_{TOA}/dT$ is reduced. This implies that insufficient averaging of surface data contributes to the observed SW absorption discrepancy. Reexamination of the observational data using the difference between cloud fraction estimated from satellite and surface measurements as an estimate of field of view mismatch supports this hypothesis. High measured absorptance values are shown to correspond to occasions of large field of view mismatch. When such data are excluded, the difference between the linear and quadratic fits is reduced, and the slope of the best fit line becomes steeper. We conclude that averaging surface data over 3 h or less is not always sufficient to eliminate sampling issues. However, the possibility that shortcomings of the RTMs contribute to the discrepancy in SW absorption values cannot be excluded.

Citation: Parding, K., L. M. Hinkelman, T. P. Ackerman, and S. A. McFarlane (2011), Shortwave absorptance in a tropical cloudy atmosphere: Reconciling calculations and observations, *J. Geophys. Res.*, *116*, D19202, doi:10.1029/2011JD015639.

1. Introduction

[2] Solar absorption in the atmosphere occurs from a combination of gaseous absorption, primarily by water vapor; aerosol absorption, primarily by carbonaceous material and wind-blown dust; and cloud hydrometeors, either liquid or ice. Gaseous absorption in the noncloudy sky is well understood. Calculations and measurements of broadband fluxes in the noncloudy sky typically agree to within a few percent with the major uncertainties coming from aerosol properties and measurements of the water vapor profile itself [see, e.g., *Conant et al.*, 1998]. Aerosol absorption is highly variable because aerosol optical depth and composition are highly variable [e.g., *Clarke and Kapustin*, 2002; *Sasheeth and Krishna Moorthy*, 2005]. Cloud absorption is a function of cloud optical depth, vertical location, geometric thickness, and solar zenith angle [e.g., *Stephens and Webster*, 1979; *Lubin et al.*, 1996; *Ramaswamy and Freidenreich*, 1998]. Because of this complexity, atmo-

[1]Geophysical Institute, University of Bergen, Bergen, Norway.
[2]Joint Institute for the Study of the Atmosphere and Ocean, University of Washington, Seattle, Washington, USA.
[3]Climate Physics Group, Pacific Northwest National Laboratory, Richland, Washington, USA.

0148-0227/11/2011JD015639

spheric absorption in the presence of clouds has proven difficult to understand.

[3] Several studies in the mid-1990s showed significantly higher SW cloud absorption from observations than predicted by theory [*Cess et al.*, 1995, 1996; *Pilewskie and Valero*, 1995; *Ramanathan et al.*, 1995]. There had been earlier contradictory reports regarding cloud SW absorption [*Stephens and Tsay*, 1990], but the magnitude of the discrepancies found in these later studies was unprecedented. The understanding of radiative transfer in clouds was questioned and some claimed that radiative transfer models (RTMs) were seriously and fundamentally flawed [*Ramanathan et al.*, 1995]. Others suggested that the excess (or "anomalous") absorption was a result of observational errors and data processing [*Francis et al.*, 1997; *Imre et al.*, 1996; *Barker and Li*, 1997]. Still other groups found little or no support for excess cloud absorption compared to RTMs [*Francis et al.*, 1997; *Li et al.*, 1999; *Sengupta and Ackerman*, 2003; *Ackerman et al.*, 2003]. *Melnikova and Vasilyev* [2005] provide a comprehensive overview of studies concerning anomalous cloud absorption.

[4] *Cess et al.* [1995] compared atmospheric absorption from collocated surface and TOA satellite observations at five locations to general circulation model (GCM) output and found that the observations "showed significant solar absorption by clouds, resulting in about 25 W m^{-2} more global mean absorption by the cloudy atmosphere than predicted by theoretical models." Although 25 W m^{-2} is a small fraction of the global average insolation, a difference of this magnitude has serious implications for Earth's climate. Estimates of cloud-induced absorptance indicated that the GCMs underestimated the absorption in clouds by around 40%.

[5] Suggested explanations for the anomalously large observed SW absorption in clouds include effects of cloud morphology and the plane parallel cloud assumption used in conventional models. *Byrne et al.* [1996] showed that broken clouds can cause SW absorption to exceed that predicted by conventional models that treat clouds as homogenous. The difference was explained by longer average photon path lengths in heterogeneous cloud fields. These simulations were performed with a single set of tropical atmospheric profiles, so the results are not necessarily valid for all conditions. *Pilewskie and Valero* [1995] used data from airplane measurements for a similar analysis, which yielded comparable results. However, more recent airplane measurements performed in maritime cumulus clouds [*Asano et al.*, 2000] have found that observed absorption agrees well with model predictions. *Ackerman et al.* [2003] analyzed three ARESE II cloudy-sky cases and found that the difference between the observed and modeled absorption in the clouds were within the uncertainty of the measurements and the RTM. Using a Monte Carlo RTM, *O'Hirok and Gautier* [1998] demonstrated that SW absorption can be underestimated when the three-dimensional structure of clouds is neglected, causing biases as large as 10%. Other model studies indicate that microphysical processes are able to produce noticeable excess absorption only when large concentrations of atmospheric aerosols are assumed [*Melnikova and Vasilyev*, 2005].

[6] Another hypothesis is that imperfect measurement techniques and methods of obtaining values of SW absorption from measurements are the main causes of observation-model absorption discrepancies [*Stephens and Tsay*, 1990; *Pilewskie and Valero*, 1995; *Francis et al.*, 1997; *Imre et al.*, 1996; *Barker and Li*, 1997]. Differences between the spatial and temporal sampling of TOA and surface measurements introduce uncertainty to the absorption computed by combining these values. The fact that typical satellite measurements have coarser spatial resolution than an upward facing pyranometer at the surface is normally addressed by averaging the surface data, which generally have higher temporal resolution than satellite data, over time. This method is based on the assumption that the time average of the surface data is, in a statistical sense, equivalent to the instantaneous spatial average within the satellite grid box. However, this assumption may not always hold. The analytical methods used to quantify cloud-induced absorption in several studies that found large discrepancies between models and observations [*Cess et al.*, 1995, 1996; *Pilewskie and Valero*, 1995; *Ramanathan et al.*, 1995] have been shown to be sensitive to sampling issues and details of the analysis [*Imre et al.*, 1996; *Barker and Li*, 1997]. Applying these methods blindly can lead to false conclusions of anomalous absorption.

[7] The objective of this study is to investigate in detail how observed SW absorption compares to RTM output in the presence of clouds. Data from Manus Island (2°S, 147°E) in the tropical western Pacific (TWP) are employed. This location was chosen primarily because the atmospheric conditions that affect SW absorptance, such as humidity and aerosol content, have relatively little variability there. Two satellite data sets, one set of surface observations, and three RTMs are used, so that common tendencies can be assumed to be robust rather than merely due to the choice of data. In addition, the various data sets are carefully examined for consistency and credibility before being compared. Nevertheless, differences between the measured and modeled absorption values are found. Causes of these observed differences are explored with a focus on data sampling issues.

2. Method

2.1. Theoretical Basis of Column Absorption Estimation and Analysis

2.1.1. Estimating Column SW Absorption

[8] The SW radiative flux absorbed within an atmospheric column, F_A, can be expressed as

$$\begin{aligned} F_A &= F^{\downarrow}_{TOA} - F^{\uparrow}_{TOA} - F^{\downarrow}_{sfc} + F^{\uparrow}_{sfc} \\ &= F^{\downarrow}_{TOA} - F^{\uparrow}_{TOA} - F^{\downarrow}_{sfc}\left(1 - \alpha_{sfc}\right), \end{aligned} \tag{1}$$

where $F^{\downarrow}_{TOA}$, $F^{\uparrow}_{TOA}$, $F^{\downarrow}_{sfc}$, and $F^{\uparrow}_{sfc}$ are the downwelling and upwelling SW fluxes at the TOA and surface, and $\alpha_{sfc} = F^{\uparrow}_{sfc}/F^{\downarrow}_{sfc}$ is the surface albedo. It is implicitly assumed that the net horizontal SW flux divergence is zero. To estimate column SW absorption, the downwelling and upwelling SW fluxes at the TOA and surface are required. These fluxes can be obtained from observations or radiative transfer models.

[9] SW fluxes have strong diurnal cycles. When looking at instantaneous values or averages over a time interval shorter than a day, absolute quantities can be difficult to interpret. Normalizing the SW fluxes with respect to the TOA insolation significantly reduces the time of day

Table 1. Summary of Radiometric Data Sources Used in This Study[a]

Data Set	Type	Dates Available	Sample Frequency
	Observations		
ARM	Broadband surface measurements	Jan 1999 to Jun 2006	1 min
GMS	Geostationary satellite, narrowband measurements	Jun 1999 to May 2003	1 h
CERES	Polar orbiting satellite, broadband measurements	Mar 2000 to Jun 2006	24 h
	Models		
ARM RT	Two-stream RTM, surface-measured inputs	Apr 2000 to Sep 2000, Apr 2003 to Sep 2006	1 min
SARB	Two-stream RTM, satellite-based inputs	Mar 2000 to Jun 2006	24 h
Model B	Empirical RTM, satellite-based inputs	Mar 2000 to Jun 2006	24 h

[a]ARM, Atmospheric Radiation Measurement; GMS, Geostationary Meteorological Satellite; CERES, Clouds and the Earth's Radiant Energy System; ARM RT, ARM radiative transfer; SARB, Surface and Atmospheric Radiation Budget; RTM, radiative transfer model.

dependence, thus facilitating the analysis of results. The normalized quantities TOA albedo or reflectance (α_{TOA}), transmittance (T), and absorptance (A), are defined as

$$\alpha_{TOA} = \frac{F^{\uparrow}_{TOA}}{F^{\downarrow}_{TOA}}, \tag{2}$$

$$T = \frac{F^{\downarrow}_{sfc}}{F^{\downarrow}_{TOA}}, \tag{3}$$

$$A = F_A / F^{\downarrow}_{TOA} = 1 - \alpha_{TOA} - \left(1 - \alpha_{sfc}\right) T. \tag{4}$$

2.1.2. Relations Among TOA Albedo, Absorptance, and Transmittance

[10] *Cess et al.* [1996] and *Pilewskie and Valero* [1995] used the slope of the best fit line of TOA albedo versus transmittance ($d\alpha_{TOA}/dT$) as an indicator of cloud absorption, arguing that increasing cloud absorption corresponds to a decrease in the magnitude of $d\alpha_{TOA}/dT$ (note that $d\alpha_{TOA}/dT$ is always negative) and that failure of samples of α_{TOA} and T to fall in a straight line is a sign of TOA and surface mismatch. Here we examine the relationships among α_{TOA}, T, and A in some detail to clarify this approach.

[11] The column SW absorptance can be related to $-d\alpha_{TOA}/dT$ by taking the derivative of equation (4) with respect to transmittance, assuming that α_{sfc} is independent of T. This yields

$$-\frac{d\alpha_{TOA}}{dT} = \left(1 - \alpha_{sfc}\right) + \frac{dA}{dT}, \tag{5}$$

[12] For a column of cloudy air, absorptance is small relative to the sum of transmittance and reflectance. As cloud coverage increases, transmittance decreases monotonically (for a fixed cloud type) while reflectance increases. Absorptance changes with increasing cloud coverage are therefore small and somewhat random, although there is a tendency toward slightly greater absorptance in cloudy columns. This result arises because (1) water vapor is the dominant absorber and absorbs roughly the same amount of solar energy whether clouds are present or not and (2) clouds redistribute absorption in the vertical column by scattering but have only about a 10%–15% effect on total absorption depending on whether they are high or low in the atmosphere. This is particularly true in the tropics, where the precipitable water column is large (between 4 and 6 cm) [*McFarlane et al.*, 2008]. To first order, then, dA/dT can be taken to be zero, particularly when averaged over all types of cloud conditions. Equation (5) then implies that the slope $d\alpha_{TOA}/dT$ is equal to $(1 - \alpha_{sfc})$. The second-order approximation is to let dA/dT equal a constant, assuming that decreasing transmission produces slightly increasing absorption. *Cess et al.* [1996] and *Pilewskie and Valero* [1995] implicitly assume that A is linearly related to T or $dA/dT = C_A$.

[13] GCMs produce a linear relation between α_{TOA} and T, but collocated satellite- and surface-based observations may exhibit a nonlinear relation. When the distribution of observational data in the α_{TOA} versus T plot is such that the data fit a parabola better than a line, the slope of the linear fit is reduced, and the small slope can be falsely interpreted as a sign of anomalous cloud absorption [*Imre et al.*, 1996; *Barker and Li*, 1997]. Assuming that the relationship between A and T, and thus α_{TOA} and T, is linear (as predicted by current 1-D radiative transfer models), any deviation from linearity in modeled or measured values of column radiation must be caused by an erroneous relationship among the variables. If A is estimated from separate measurements of TOA and surface fluxes, the simplest explanation is that the two sets of measurements do not correspond to each other as closely as needed for this computation. Hence, it is reasonable to interpret nonlinearity in plots of α_{TOA} versus T for observational data as indicative of mismatch in the TOA and surface measurements. However, the possibility that natural processes may cause the relationship between α_{TOA} and T to be nonlinear should not be discounted. As mentioned by *Cess et al.* [1996], three-dimensional (3-D) radiative transport effects can produce nonlinearities resembling those from sample mismatch when the cloud field is broken.

[14] If the nonlinearity in the (α_{TOA}, T) relation is caused by the field of view mismatch of TOA and surface instrumentation, averaging the surface data over time may compensate for the narrower field of view of the surface-based pyranometer. If curvature remains after such averaging, then the slope method cannot be used to infer increases in SW column absorption due to clouds.

2.2. Data Sets

[15] The data sets used in this study are listed in Table 1. The observations are described in further detail in section 2.2.1, and the radiative transfer models in section 2.2.2.

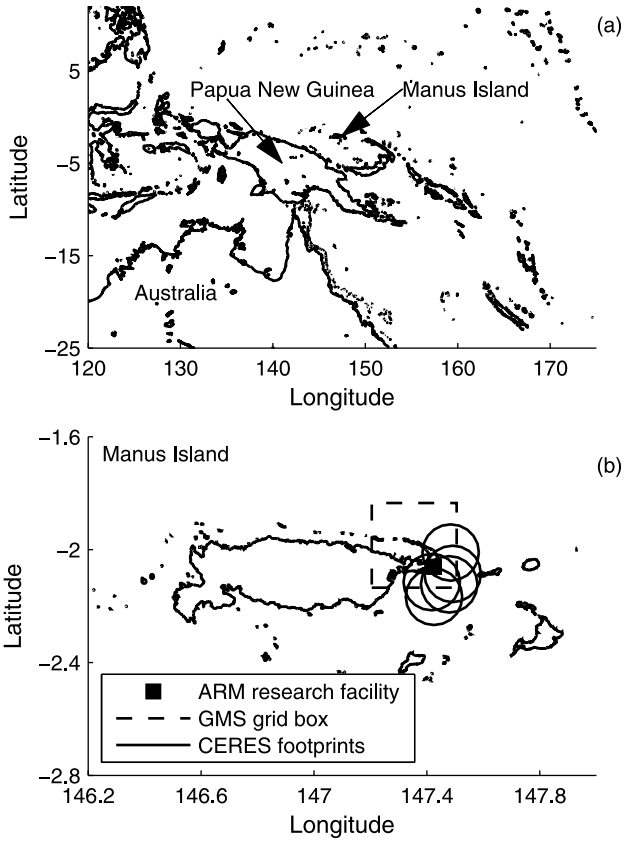

Figure 1. (a) Location of Manus Island in the tropical western Pacific. (b) Map of Manus Island. The Atmospheric Radiation Measurement (ARM) facility is located on Los Negros Island, east of the main island. The locations and approximate size of the central Geostationary Meteorological Satellite (GMS) grid box and a sample of Clouds and the Earth's Radiant Energy System (CERES) nadir footprints are included.

2.2.1. Observations

[16] The U.S. Department of Energy's Atmospheric Radiation Measurement (ARM) Program was founded in 1989 and provides the scientific community with continuous atmospheric field observations. The Manus ARM climate research facility was established in 1996 as the first of three ARM facilities in the tropical western Pacific region [*Mather et al.*, 1998]. Instruments at the Manus site include broadband radiometers, radiosondes launched twice daily, a microwave radiometer, and active remote sensing instruments. ARM 1 min surface data from Manus, including SW fluxes measured by broadband radiometer with a hemispheric field of view [*Stoffel*, 2004], have been processed and analyzed by Charles N. Long at the Pacific Northwest National Laboratory, from whom the data were obtained. The cloud fraction is estimated from measurements of total and diffuse SW irradiance and is valid for a hemispheric 160° field of view [*Long et al.*, 2006]. The observed upwelling SW flux is not representative of the whole island or the surrounding ocean, as the downward facing radiometer observes only a small surface area. Since the ARM site is located on the eastern end of the island, as seen in Figure 1, and the satellite grid boxes contain a large percentage of open water, the upwelling SW flux at the surface has instead been estimated by multiplying the observed downwelling surface flux by a fixed surface albedo value of 0.05, corresponding to the average broadband albedo of the tropical ocean surface [*Payne*, 1972]. *Chiu et al.* [2004] looked at the effect of surface albedo on absorption estimates through sensitivity calculations and found the effects to be negligible compared to uncertainty in other variables.

[17] The Geostationary Meteorological Satellite (GMS) series is operated by the Japanese Meteorological Agency [*Kisho Eisei Senta*, 1997]. GMS-5 was launched into a geostationary orbit above 0°N, 140°E in March 1995 and was taken out of service in May 2003. The Visible and Spin Scan Radiometer (VISSR) on board the GMS-5 measured upwelling radiative energy at a spatial resolution of 1.25 km in the visible channel (0.55 to 0.90 μm). GMS data have been processed at the NASA Langley Research Center for the ARM Program [*Minnis et al.*, 1993, 1995]. The GMS-5 0.30° layered bispectral threshold method (LBTM) ARM cloud product for Manus includes broadband SW albedo at the top of atmosphere (TOA) and solar zenith angles (SZAs) from which the downwelling and upwelling SW flux at the TOA can be calculated. Values are provided hourly for each of nine contiguous 0.3° × 0.3° grid boxes. Unless otherwise indicated, the value for the center grid box, which is closest to the ARM research facility, is used in this study. The nominal time stamp included in the GMS data product is not the exact time of the measurement. Comparing SZAs included in the GMS data files with SZAs calculated from the nominal time and the location of the grid box, there is a consistent difference of approximately +10 min. In this work, we have not corrected the time stamps because the offset was found not to affect the SW flux and column absorption comparisons significantly.

[18] Clouds and Earth's Radiant Energy System (CERES) instruments are carried by the polar-orbiting spacecraft Terra (nominal equator crossing time: 10:30 local time (LT)). Terra was launched in 1999 as part of NASA's Earth Observing System (EOS) program for long-term, global observations of the earth and atmosphere. The CERES SW radiometer band spans 0.2–5 μm and has a nadir footprint size of approximately 20 km. The Moderate Resolution Imaging Spectroradiometer (MODIS), which is also on board Terra and has a spatial resolution of about 1 km, is used for cloud detection within the CERES footprints. The CERES observation (footprint) closest to the ARM facility at Manus was chosen for each satellite overpass time.

[19] Satellite measurements of SW radiation undergo several conversions. First the raw detector counts are converted to radiance. Then, if the observations are made in limited wavelength bands (as for GMS-5), the radiance is converted from narrowband to broadband. Finally, a bidirectional reflectance distribution function (BRDF) is applied to the radiance to convert it to a SW flux. In every step of the data processing, uncertainties are added. The BRDFs used for CERES have been validated by *Loeb et al.* [2007]. *Minnis et al.* [1993] include a brief description of the angular dependence of the radiance and the radiance-to-flux conversion for their algorithm.

2.2.2. Radiative Transfer Models

[20] Following the method of *Mather et al.* [2007], ARM surface observations from Manus were used to compute

atmospheric absorption and heating rate profiles using the Fu-Liou radiative transfer code [*Fu and Liou*, 1992]. We refer to this data set as ARM RT. Inputs to the radiative transfer model include surface albedo and vertical profiles of temperature, water vapor, and cloud properties. In the current version of the ARM RT data set (version 5), the surface albedo at Manus is fixed to 0.05, aerosols are not included as input, and the profiles of temperature and water vapor are obtained from the ARM merged sounding value added product [*Troyan*, 2010]. Vertical profiles of cloud liquid water content, ice water content, and particle size are derived from radar reflectivity and temperature profiles as by *Mather et al.* [2007], but at 1 min resolution. Estimates of the visible optical depth for liquid water and ice clouds (τ_{liq} and τ_{ice}) are determined from the retrieved water content and particle size. Each 1 min sample is assigned a cloud flag: 0 if both τ_{liq} and τ_{ice} are zero, indicating cloud-free conditions, and 1 otherwise. Cloud frequency over a given averaging period is calculated as the time average of the cloud flag. Manus ARM data from 2000 and 2003–2006 were processed. The long period of missing data is due to the Manus radar being inoperative during parts of this period and concerns about data quality during the remainder of the period. ARM RT output includes both surface and TOA SW fluxes computed at 1 min intervals. Because the vertical profile of cloud properties used in the ARM RT calculations are derived from the radar, which has a narrow field of view, the output data (SW fluxes, cloud optical depth) are representative of a narrow column over the observation site.

[21] The CERES Clouds and Radiative Swath (CRS) data product includes surface SW fluxes estimated by two different RTMs. The first is the Surface and Atmospheric Radiation Budget (SARB) algorithm [*Wielicki et al.*, 1998; *Rutan et al.*, 2009]. Like the ARM RT model, SARB is based on the Fu-Liou radiative transfer code, but uses inputs derived from satellite measurements. After applying the SARB algorithm to measurements of cloud and aerosol properties from MODIS and atmospheric characteristics from GEOS-4.0 [*Bloom et al.*, 2005], the model output is tuned to CERES TOA observations by adjusting one or more of the input parameters. SARB output includes both TOA and surface SW fluxes. The second radiative transfer model is the Langley parameterized shortwave algorithm (LPSA) [*Gupta et al.*, 2001; *Kratz et al.*, 2010], referred to as Model B in CERES CRS files. Model B uses a simple parameterization to produce surface SW fluxes only. When estimating SW absorption from Model B, we couple the model surface fluxes with simultaneous CERES TOA observations.

2.3. Site Description

[22] The site chosen for this study is Manus Island, Papua New Guinea, in the tropical western Pacific (Figure 1). Manus is approximately 100 km long (E-W) and 30 km wide (N-S) and is situated in the Pacific Warm Pool [*Mather et al.*, 1998]. The TWP is a convectively active region where cloud fields are complex and cloud formation is easily triggered because of high atmospheric moist static energy content. Large scale oscillations such as the El Niño–Southern Oscillation (ENSO) and the Madden-Julian Oscillation (MJO) influence the weather by suppressing or encouraging cloud formation [*Mather*, 2005]. Despite the complexity of cloud fields in the TWP, there are several good reasons to work with SW radiation data from Manus. Some of the original studies showing anomalous absorption were done using observations from the tropics [*Ramanathan et al.*, 1995]. There is little variability and seasonal dependency in the climate of Manus: there are no dry or rainy seasons and the temperature has no clear seasonal cycle [*Mather et al.*, 1998]. The Manus ARM site experiences convection throughout the year, although there is some seasonality in the sources and characteristics of the clouds [*Mather*, 2005]. Oceanic sites provide dark uniform surfaces, which simplifies both the computation of upward SW fluxes and satellite detection of clouds. In the tropics, land surfaces are generally dark as well, so that the surface albedo within a satellite grid box covering a tropical island is expected to be small and relatively homogenous. The viewing zenith angle (VZA) is the angle between the line of sight of a satellite and the local zenith. For large VZAs, the BRDF is both more important and complex than at smaller VZAs. A slanted view also increases the size of satellite grid boxes and changes the view of the clouds. When using data from a geostationary satellite, located over the equator, choosing a low-latitude site minimizes the problems of high VZAs.

[23] Another reason to focus on the tropical western Pacific in this study is to limit aerosol absorption. Aerosol optical depths over the Pacific Ocean are expected to be on the order of 0.07–0.08 [*Smirnov et al.*, 2002]. However, preliminary work by A. Vogelmann (Aerosol radiative effects in the tropical western Pacific, paper presented at Twelfth ARM Science Team Meeting, St. Petersburg, Florida, 2002) indicated that continental-sized particles are present at Manus much of the year, with the largest optical depths occurring from August to October because of biomass burning. Particularly high optical depths were observed under the strong El Niño conditions of 1997 (Vogelmann, presented paper, 2002; J. D. Spinhirne et al., Optical properties of the 1997 smoke event at the ARM tropical western Pacific site, paper presented at Eighth ARM Science Team Meeting, Tucson, AZ, 1998.) To assess the aerosol properties during the period considered here, we examined aerosol optical depth (τ_{aer}) retrieved from the ARM multifilter rotating shadow band radiometer under clear sky conditions. Daily average τ_{aer} was calculated for all days in the ARM RT data set that had at least 10 min of valid τ_{aer} data (20% of days). The mean daily τ_{aer} was 0.057, with a standard deviation of 0.037, showing that the conditions at Manus were quite clean during this period. For this reason, we do not specifically consider the variability of aerosol absorption in this study. However, the time-varying effect of aerosols is included in the observations and the SARB radiative transfer model. Aerosols are also included as static parameters in Model B but are omitted from the ARM RT computations.

[24] The ARM facility at Manus is located on Los Negros island (2.06°S and 147.42°E), just east of the main island. The nominal center of the GMS middle grid box at Manus is 1.98°S and 147.35°E. Figure 1b shows the approximate locations of the ARM facility and GMS center grid box as well as a sample of CERES footprints.

2.4. Data Preparation

[25] Observational estimates of column SW absorption were obtained by combining collocated satellite and surface measurements, yielding two data sets designated as GMS/ARM and CERES/ARM. To compensate for the difference in field of view between the satellite and surface instruments, the surface data were averaged over a time interval t_{avg}. (This procedure is discussed further in section 2.5.) Averaging times from 30 min up to 3 h were tested (see discussion in section 5.1). Unless otherwise indicated, an averaging interval of 60 min has been used. If more than 10% of the observations within an averaging interval were missing, the entire interval was discarded. Data from before 0900 LT and after 1500 LT were excluded to avoid the problems associated with large SZAs. CERES measurements with VZA > 50° were also excluded. GMS makes hourly observations and, for the longer surface measurement averaging times, time averages of these TOA observations can also be employed instead of single, instantaneous measurements. Both alternatives have been tested, but unless otherwise stated, instantaneous GMS observations have been used.

[26] Atmospheric absorption was computed for the SARB and ARM RT model output using the TOA and surface upward and downward fluxes, as shown in equation (1). The ARM RT model output, which has a 1 min time resolution, was averaged over 60 min to match the ARM surface data. (Trials covering the range of 30 min to 3 h showed little impact on the result.) The absorption estimate for Model B combined TOA CERES observations with modeled upwelling and downwelling fluxes at the surface. Each daily CERES observation yielded one instantaneous sample of SARB and Model B output.

[27] SW TOA albedo and column transmittance and absorptance were calculated for all data sets following equations (2), (4), and (3), respectively.

[28] When all data sets were compared as a group, the GMS and CERES sampling times were required to match to within 30 min. Instances when all observational and modeled data sets are available simultaneously are few (53) because of the limited overlap of CERES measurements and ARM RT computations. To increase the number of sample points, comparisons involving only one of these two data sources were sometimes made. In this case, SARB and Model B output were compared to CERES/ARM and GMS/ARM data recorded between 1030 LT and 1130 LT from March 2000 to May 2003. This yields about 480 matched samples depending on the averaging period used for the surface data. Separate comparisons between ARM RT and GMS/ARM values included about 750 matches between 0900 LT and 1500 LT from April 2000 to May 2003. Comparing all available overlapping ARM RT and CERES/ARM data results in about 1080 matching samples from between 1030 LT and 1130 LT, from April 2000 to June 2006.

2.5. Sampling Issues

[29] Satellite and surface measurements of SW radiative fluxes have different spatial resolutions and viewing geometries. Satellite samples cover a large area (CERES nadir footprint size: ~20 km, increasing with VZA; GMS grid box size: ~30 km) and report fluxes as averages over all cloud observation pixels within the sampling area. An upward facing pyranometer at the surface has a hemispheric view, but still detects radiation from a smaller portion of the atmospheric column than is included in the GMS grid boxes or CERES footprints. Since surface measurements are typically made more frequently than TOA observations, it is common practice to compensate for the field of view mismatch by temporally averaging the surface data. This implies that the spatial average over the satellite footprint at an instant of time is equivalent to the time average over the smaller area covered by the surface instrument. This is known as the ergodic assumption [*Peixoto and Oort*, 1992]. For a statistically stationary, ergodic system, the instantaneous average over all members of an ensemble can be replaced by the time average of a single member of the ensemble over a sufficient time period. This requires that the measured variable "passes through all states available to it" over the averaging period [*Peixoto and Oort*, 1992].

[30] Using collocated surface and TOA observations from a site in Wisconsin, *Long and Ackerman* [1995] showed implicitly that temporal and spatial averaging are comparable. *Cess et al.* [1996, p. 23,301] demonstrated through explicit comparisons that "in a statistical context, temporally averaging the surface measurements can be equivalent to spatially averaging them over the satellite grid" for the same Wisconsin data. An averaging time of 60 min was found to be sufficient in this case. Nevertheless, it is not obvious this would also be true for a site in the TWP because the atmospheric dynamics of the midlatitudes and the tropics are very different. Since the timescale and spatial scale of cloud formation processes are not the same, an averaging time that is adequate in Wisconsin may be inappropriate at Manus.

[31] Under clear or overcast conditions, satellite and surface observations should be similar. In a scene of broken or scattered clouds, the cloud cover over the surface radiometer may differ from the rest of the satellite field of view. If clouds pass through the footprint in a time shorter than the averaging time (i.e., if the wind speed is high enough), or if the cloud lifetime is shorter than the averaging time and the probability of cloud formation is evenly distributed within the footprint, then a time average of surface observations could be used as a substitute for the instantaneous spatial average. We examine the validity of the ergodic assumption and the appropriate averaging time of the surface data at Manus later in this paper.

3. Evaluation of the Data Sets

[32] Before analyzing the various column absorption values, we assessed the input data sets for consistency, significant deviations, and spurious values. The satellite data products are compared in section 3.1, the model outputs in section 3.2, and the observational and model data sets to each other in section 3.3.

[33] The statistical measures used to characterize the data are the mean value and standard deviation (SD), and, when comparing two data sets, the bias (mean difference), root-mean-square difference (RMSD), and Pearson correlation coefficient (R). The Kolmogorov-Smirnov test is applied to determine whether the bias is statistically significant. This

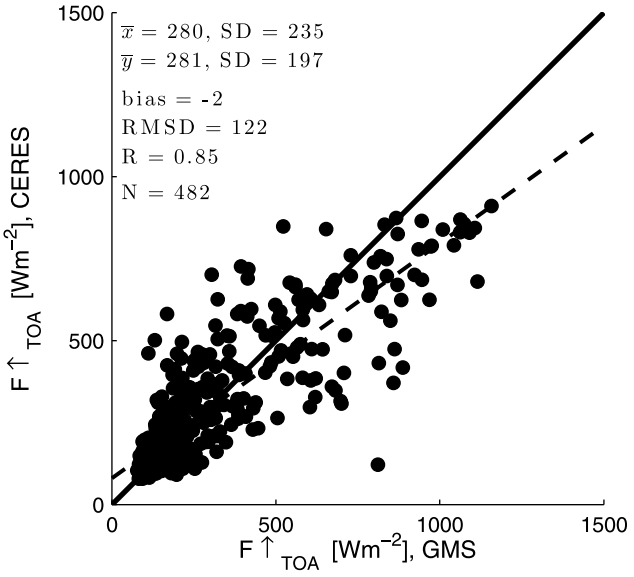

Figure 2. Comparison of $F\uparrow_{TOA}$ from the GMS and CERES satellite data sets. The statistical measures included are the mean value and SD of $F\uparrow_{TOA}$ for each data set (x = GMS, y = CERES) and the bias, root-mean-square difference, and correlation coefficient (R) between the data sets. N is the sample size. In the figures, bold values indicate a statistically significant difference at the 5% level. Best fit (dashed) and one-to-one (solid) lines are also plotted.

significance test is chosen because it does not require the data to be normally distributed.

3.1. CERES and GMS Satellite Observations

[34] A comparison of upwelling SW fluxes at the TOA obtained from the GMS and CERES satellite observations is shown in Figure 2. These fluxes are found to be highly correlated (R = 0.85), with a bias and RMSD of −2 and 122 W m^{-2}, respectively. Because the GMS data have a coarser base resolution, cover a different spatial area, and have a slightly different sampling time than the CERES footprints (here the maximum allowed time stamp difference is 15 min), exact agreement is not expected. Some differences due to measurement uncertainties and the conversion from the measured radiances to fluxes are also expected. The small bias between the data sets indicates that that such uncertainties are mostly random in nature.

[35] Despite the lack of a bias, higher maximum GMS upwelling fluxes are observed. The maximum CERES $F\uparrow_{TOA}$ is about 900 W m^{-2}, whereas the GMS $F\uparrow_{TOA}$ reaches values well over 1000 W m^{-2}. In terms of TOA albedo, the maximum values are approximately 0.75 and 0.95 for CERES and GMS, respectively. Since TOA albedos generally do not surpass 0.8 even for deep convective clouds, the high values from the GMS are clearly excessive. Because the CERES instrument is better calibrated than meteorological satellites, makes broadband measurements, and uses newer BRDFs computed from its own observations, the CERES results are expected to be more accurate.

3.2. Radiative Transfer Model Data Sets

[36] Figure 3 shows that the surface fluxes from the CERES Model B and SARB products are nearly identical, with a high correlation (R = 1.00) and small bias and RMSD (−1 and 19 W m^{-2}, respectively). On the basis of this comparison, the tuned SARB model output is assumed to be representative of the modeled CERES SW fluxes. For this reason, only the tuned SARB values are employed in the remaining analysis.

[37] The level of agreement between the surface downwelling fluxes from ARM RT and SARB (Figure 4) is not as high, with a much larger bias (−92 W m^{-2}) and RMSD (173 W m^{-2}). However, the correlation is rather strong (R = 0.89). Correspondingly, comparison of the TOA upwelling fluxes from ARM RT and SARB yields a large positive bias (59 W m^{-2}) and large RMSD (142 W m^{-2}) but high correlation (R = 0.89). Compared to SARB, the ARM RT surface fluxes are consistently lower, especially in the range below 500 W m^{-2}. The ARM RT upwelling TOA SW fluxes are higher than the corresponding SARB fluxes, most notably above 500 W m^{-2}.

[38] Although both SARB and ARM RT are two-stream models based on the Fu-Liou computational code, their inputs are quite different. In particular, SARB uses satellite-based cloud data while ARM RT comes from combined radar and lidar measurements. These active instruments observe only a narrow slice of the cloud field passing over the surface site, giving them a field of view narrower than even the surface radiometer measurements. In contrast, Model B and SARB are run using identical cloud properties. This explains why the SARB and Model B fluxes are more similar than those from SARB and ARM RT.

3.3. Comparison of Models and Observations

[39] Statistics comparing model and observational SW flux data are summarized in Table 2. A reference observa-

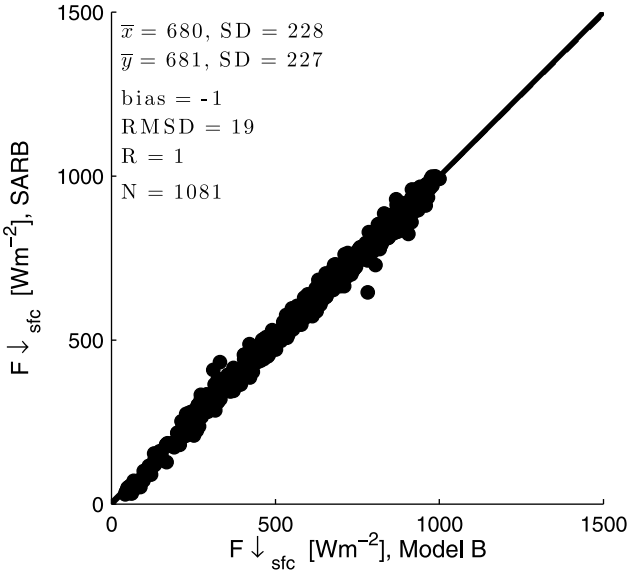

Figure 3. Comparison of $F\downarrow_{sfc}$ from CERES Surface and Atmospheric Radiation Budget (SARB) and Model B. Statistical measures are as in Figure 2.

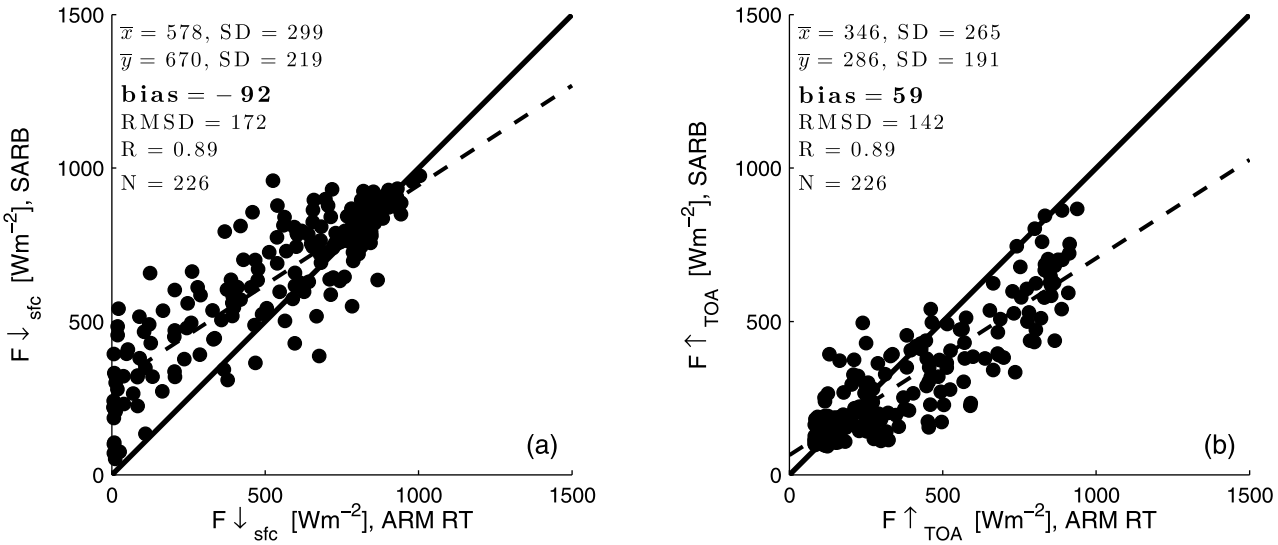

Figure 4. Comparison of shortwave (SW) fluxes from SARB and ARM radiative transfer (RT). The ARM RT data are averaged over 60 min. (a) $F\downarrow_{sfc}$ and (b) $F\uparrow_{TOA}$. Statistical measures are as in Figure 2.

tional data set (CERES for the TOA fluxes, ARM for the surface fluxes) is used for each set of comparisons. An averaging time of 60 min is applied to the ARM surface measurements. This analysis is limited to the 53 occasions for which all data sets are available (time period: March–September 2000 and May–April 2003, 10:30–11:30 LT). This results in somewhat different values than in the results discussed above, which used the maximum number of matches available for each comparison. This demonstrates the sensitivity of statistics computed for a small population to the specific samples included.

[40] The SARB $F\uparrow_{TOA}$ values are, as expected, nearly identical to the CERES satellite observations, with a correlation coefficient of 1.0 and a bias of just 7 W m^{-2}. The SARB surface SW fluxes also have a positive linear relationship with the ARM surface measurements (R = 0.89), but the bias between them is larger (14 W m^{-2}). This is not surprising for a comparison of surface- and satellite-based data. Similarly, the ARM RT TOA output, which is based on surface measurement inputs, has a strong correlation with

Table 2. Comparisons of Measured and Modeled Data Using One Data Set as a Reference[a]

	$F\uparrow_{TOA}$ (W m^{-2})		CERES Reference Data		
Data Set	Mean	SD	Bias (W m^{-2})	RMSD (W m^{-2})	R
CERES	237	169	0	0	1.00
GMS	224	209	−13	108	0.86
SARB	243	164	7	11	1.00
ARM RT	305	247	69	146	0.87
Data Set	$F\downarrow_{sfc}$ (W m^{-2})		ARM Reference Data		
	Mean	SD	Bias (W m^{-2})	RMSD (W m^{-2})	R
ARM	722	227	0	0	1.00
SARB	736	188	14	105	0.89
ARM RT	645	286	−77	141	0.92

[a]Statistical measures are as in Figure 2; 53 samples are used for all comparisons. RMSD, root-mean-square difference.

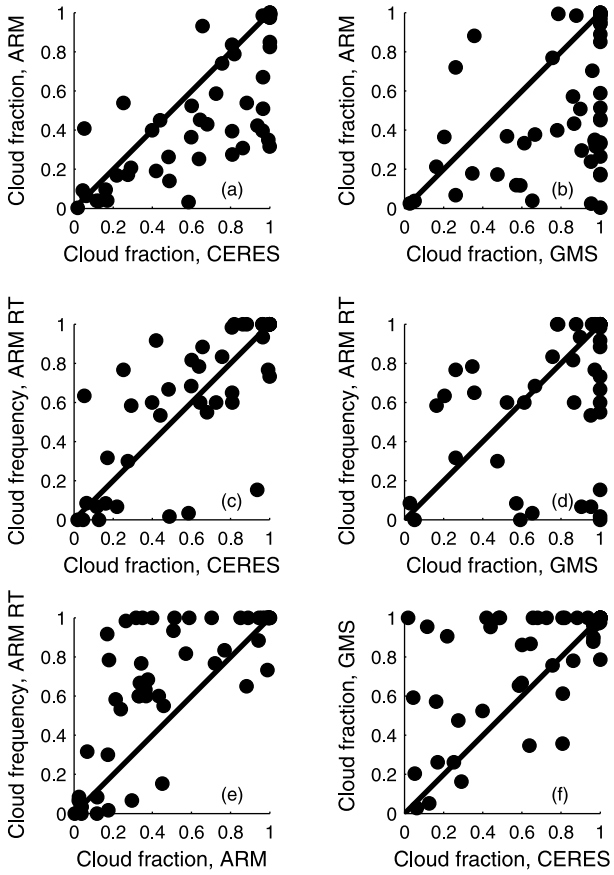

Figure 5. Comparison of cloud fraction estimates from observational and model data sets. The plots include 53 samples from the time period March–September 2000 and May–April 2003, 10:30–11:30 LT. Comparison between cloud fractions from the (a) CERES and ARM data sets, (b) GMS and ARM data sets, (c) CERES and ARM RT data sets, (d) GMS and ARM RT data sets, (e) ARM and ARM RT data sets and (f) CERES and GMS data sets.

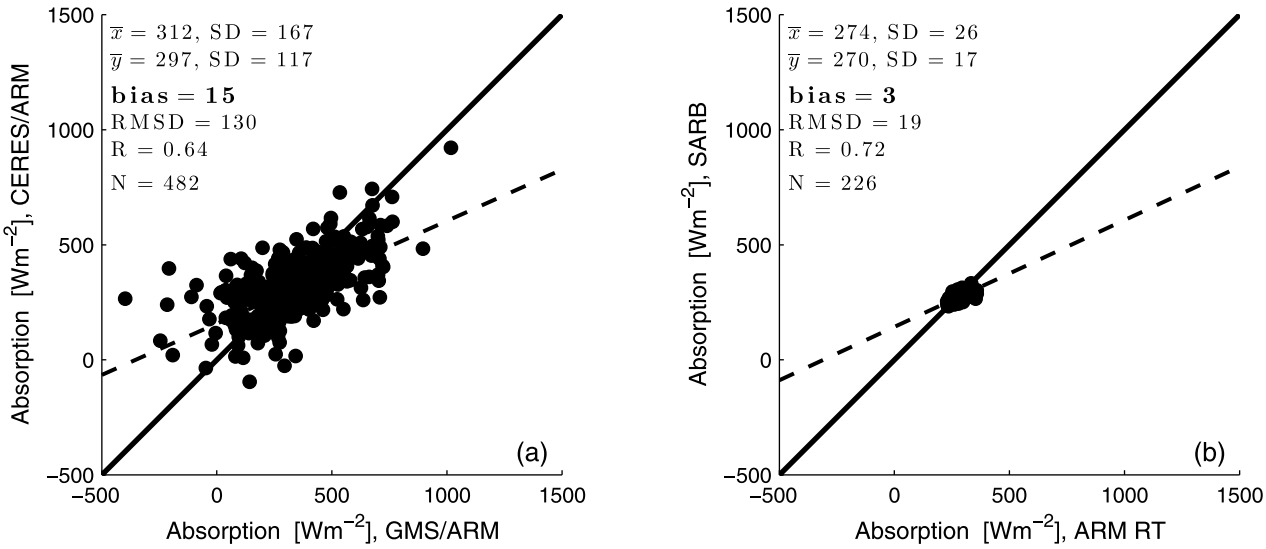

Figure 6. Comparisons of column SW absorption estimated using (a) the GMS/ARM and CERES/ARM collocated satellite and surface observations and (b) the ARM RT and SARB models. The ARM and ARM RT data are averaged over 60 min. Statistical measures are as in Figure 2.

the CERES observed TOA fluxes but a larger bias from CERES than SARB (R = 0.87, bias = 69 W m^{-2}.)

[41] It is interesting to note that the SARB model surface SW fluxes agree better with the ARM measurements than the ARM RT values do. Although the ARM observations of $F\downarrow_{sfc}$ are not used in the ARM RT computations, one would expect good agreement between the two data sets since they are based on upward looking measurements taken simultaneously at the same location and averaged over the same time periods. It is assumed that the poorer than expected agreement can be traced to sampling differences between the surface radiometer (which has a hemispheric field of view) and the narrow beams of the active remote sensors used to detect clouds above the Manus site in addition to any model errors, including omission of any 3-D radiative transfer effects.

[42] It should be noted that none of the biases found between the reference SW fluxes and the other data sets are statistically significant at the 5% level.

[43] Differences among the flux values from the various data sets may be explained in part by differences in the cloud fraction from the instruments or model inputs. Figure 5 shows scatterplots of cloud fraction values from each data set for the 53 common data samples. Only four data sets appear in this plot because the cloud amounts for SARB and the CERES observations are the same. This fact explains why the CERES and SARB TOA fluxes are so similar. The data sets rarely agree on the exact cloud amount. This can be interpreted as a sign of field of view mismatch, but the cloud fraction discrepancies may also be due to different cloud detection algorithms. GMS data show a higher overcast (cloud fraction >0.9) frequency than the other data sets, leading to a high bias in the outgoing TOA flux. The ARM data exhibit a tendency for lower cloud fraction and fewer overcast cases than the other data sets, yielding larger surface fluxes than the SARB data. The relationship between the cloud fractions for ARM RT and the other data sets is difficult to generalize since the ARM RT values tend toward the high side but also include more clear cases than any other data set. It is worth noting that most of the samples considered in this analysis are for cloudy columns.

4. Column SW Absorption

[44] Having examined the measured and modeled fluxes in some detail, we now address the question of whether significant biases between measured and modeled column absorption occur under cloudy skies at Manus Island in the tropical western Pacific. First, the paired data sets are compared in Figure 6 (observations in Figure 6a and model data in Figure 6b). Although the bias between GMS/ARM and CERES/ARM absorption values is moderate (15 W m^{-2}) the scatter between the absorption values from these data sets is large (RMSD of 130 W m^{-2}), especially compared to the mean absorption values of approximately 300 W m^{-2}. On the other hand, the absorption values from the two models are quite similar (bias = 4 W m^{-2}, RMSD = 19 W m^{-2}), despite the differences between the TOA and surface SW fluxes from these models noted above.

[45] Consistent with prior studies [*Cess et al.*, 1995, 1996; *Pilewskie and Valero*, 1995; *Ramanathan et al.*, 1995], a model-observation SW column absorption bias is found (Figure 7) when all available matches are used in each comparison. For all possible combinations of the observational and model data sets, the models give lower SW absorption values than the observations, with mean differences ranging from −13 to −32 W m^{-2}. The comparison between ARM RT and CERES/ARM data gives the smallest bias (−13 W m^{-2}). All four bias values are significant at the 5% level. The amount of data available for the ARM RT-CERES/ARM comparison is smaller than for the others and the results are likely sensitive to the exact sample population considered. For example, the 226 CERES/ARM values used in this comparison have a lower mean absorption than the 1081 values that are compared to the SARB model data. The results of the simultaneous comparison of all data sets

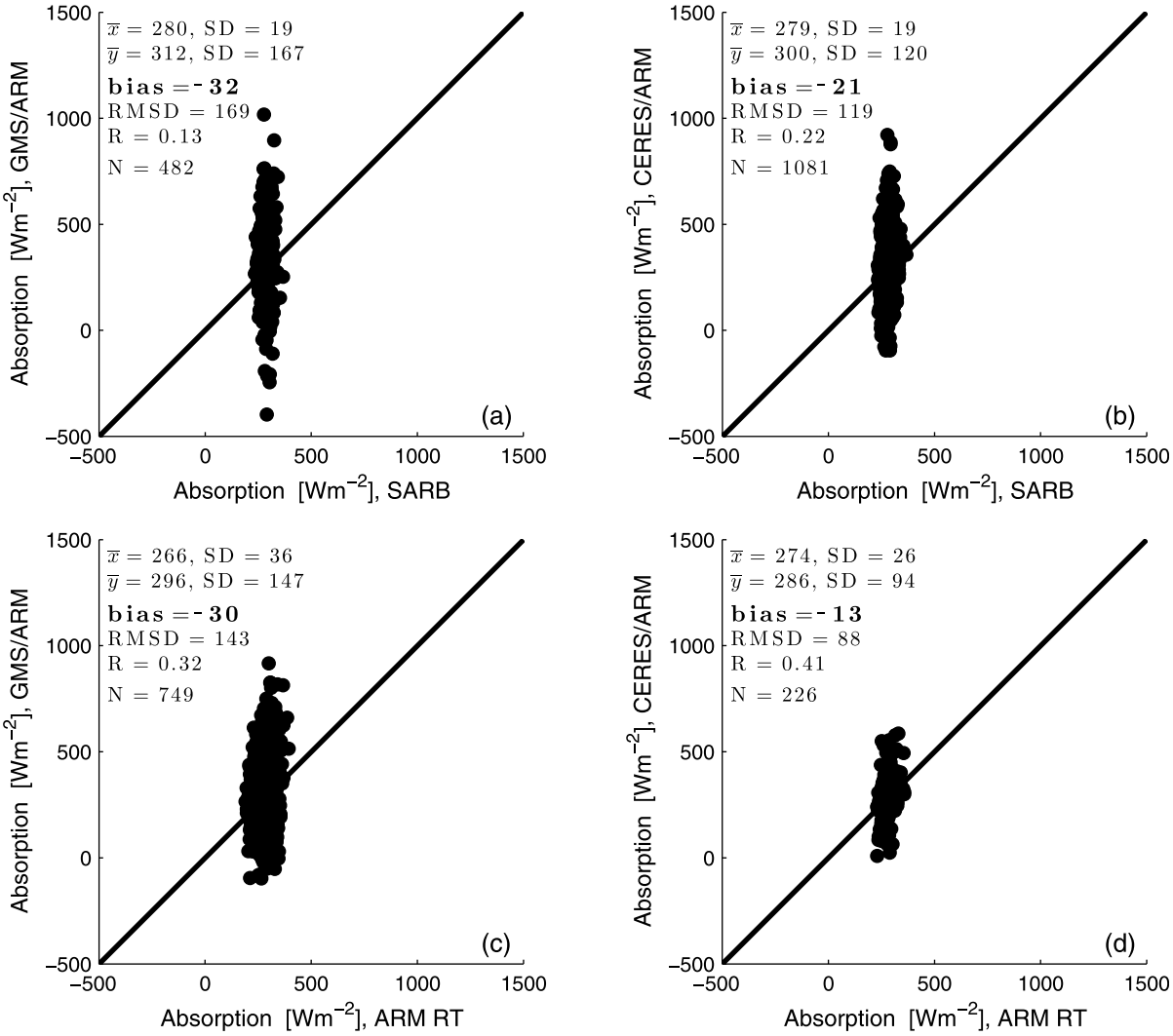

Figure 7. Comparisons between column SW absorption values obtained from collocated satellite and surface observations (GMS/ARM and CERES/ARM) and values from radiative transfer model output: (a and b) SARB and (c and d) ARM RT. The ARM and ARM RT data are averaged over 60 min. Statistical measures are as in Figure 2.

(Table 3) are based on an even smaller sample size from the same period. This comparison still shows a significant bias between the GMS/ARM and model data but only a small bias between the absorption obtained from CERES/ARM and the RTMs. A somewhat larger bias (21 W m^{-2}) between GMS/ARM and CERES/ARM is also indicated.

[46] A more striking feature of Figure 7 is the large difference in the range of SW column absorption values produced by the models and observations. The absorbed fluxes computed by the models fall within relatively narrow intervals, 270 ± 27 W m^{-2} for ARM RT and 274 ± 17 W m^{-2} for SARB, while the collocated satellite and surface observation data sets give absorption values of 312 ± 168 W m^{-2} and 297 ± 117 W m^{-2} for GMS/ARM and CERES/ARM, respectively. Clearly, the two approaches to obtaining column absorption are not equivalent. Since it is highly unlikely that natural variability in atmospheric and cloud conditions can explain relative variations of 40%–65% in total SW column absorption [*McFarlane et al.*, 2008], we consider the absorption estimated by combining satellite and surface observations to be unreliable. In section 5, we explore the reasons for this large discrepancy.

5. Analysis

[47] Figure 8 shows modeled and observed TOA and surface SW fluxes and column SW absorption for the 53 occasions when all data sets are available. The TOA and

Table 3. Comparisons of Measured and Modeled F_A[a]

	GMS/ARM			CERES/ARM		
Data Set	Bias	RMSD	R	Bias	RMSD	R
SARB	**−21**	141	0.02	0	101	0.04
ARM RT	**−21**	134	0.35	**1**	92	0.45

[a]Statistical measures are as in Figure 2; 53 samples are used for all comparisons. Bold indicates a statistically significant difference at the 5% level.

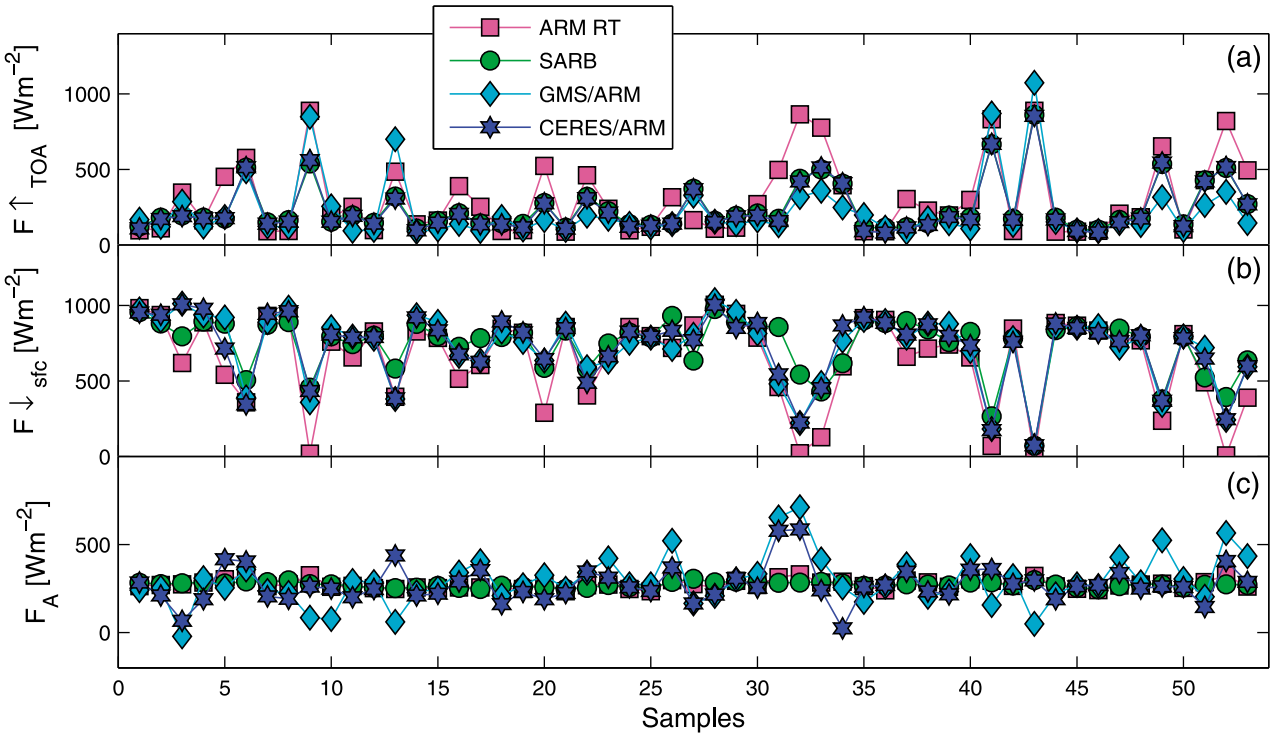

Figure 8. Time series of (a) $F\uparrow_{TOA}$ and (b) $F\downarrow_{sfc}$ and (c) column SW absorption (F_A) from the ARM RT, SARB, GMS, CERES, and ARM data sets.

surface SW fluxes from the models closely mirror each other, so that the absorption values have small variability. On the other hand, the TOA and surface observations often fail to balance each other, giving more extreme, and even negative, absorption values. The lack of symmetry between observed TOA and surface SW fluxes suggests that differences in field of view between satellite- and surface-based instruments contribute significantly to apparent absorption variability. In sections 5.1–5.3, the effects of sampling differences between surface and satellite observations are investigated. The normalized quantities TOA albedo, transmittance, and absorptance are employed in this analysis to facilitate interpretation of the results.

5.1. Effect of Averaging Time

[48] As discussed in section 2.5, temporal averaging of the surface data is usually used to compensate for field of view mismatch between satellite and surface measurements. As a first check of the effectiveness of this averaging, observed absorptance values computed using different averaging times for the surface data are compared to model output. Averaging times from 30 to 180 min are tested. The agreement between observed and modeled absorptance is found not to improve for longer averaging times. Using a longer averaging time does reduce the absorptance variability computed from observations. For GMS/ARM, the standard deviation decreases from about 60% to 45% of the mean value going from t_{avg} = 30 to 180 min. The corresponding variability reduction for CERES/ARM is from approximately 45% to 30%. Nevertheless, even for a t_{avg} of 180 min, these standard deviations are large compared to the variability of modeled absorptance (less than 10%.) In addition, the biases between the observation- and model-based absorptances increase when a longer averaging time is used, from 2%–7% at 30 min to 8%–10% at 180 min. The correlation between measured and modeled absorptance values also gets weaker with a longer averaging time.

[49] Plots of TOA albedo versus transmittance (Figures 9 and 10) are used to further investigate the effect of surface measurement averaging time on the column SW absorptance values. The slope of α_{TOA} versus T must be negative because high TOA albedo gives low transmittance and vice versa. The right end of the line (high transmittance and low TOA albedo) corresponds to clear skies. Given relatively constant atmospheric and aerosol conditions, this portion of the line will be firmly anchored, so that any change in the slope is related to behavior as cloud amount increases. A shallower slope indicates that the TOA albedo does not increase as quickly as expected when transmittance falls and can therefore be interpreted as a sign of higher SW absorptance in the presence of thick clouds. A steeper slope corresponds to less cloud absorption. Rather than relying solely on the slope as an indicator of cloud absorptance, we explicitly show the absorptance corresponding to each point in the TOA albedo-transmittance plots using a color scale. This allows the plots to be interpreted more easily, particularly when the relationship between α_{TOA} and T is nonlinear.

[50] Plots for the SARB and ARM RT models and both observational data sets are shown in Figure 9, along with linear and quadratic fits to the data. The RMSD between points on the linear fit and the quadratic fit, taken both horizontally (along constant T) and vertically (along constant α_{TOA}), is used as a measure of nonlinearity. This quantity is referred to as the linear-quadratic RMSD ($RMSD_{l-q}$). When the relationship between transmittance and TOA albedo is not linear, sampling mismatch is indi-

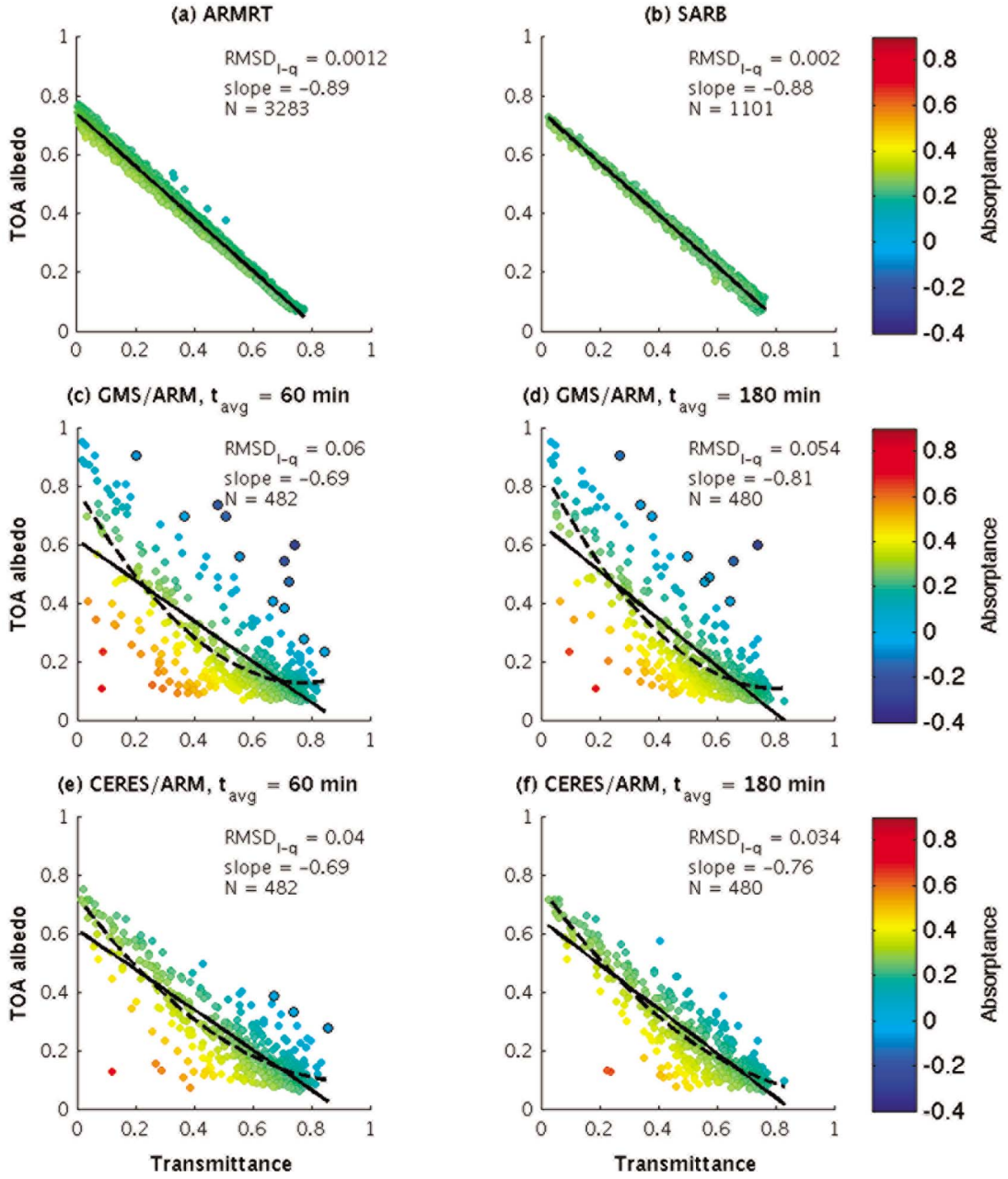

Figure 9. Plots of α_{TOA} versus T, with absorptance as a third dimension indicated by the color scale, and a linear and quadratic fit. (a) ARM RT, (b) SARB, (c) GMS/ARM with t_{avg} = 60 min, (d) GMS/ARM with t_{avg} = 180 min, (e) CERES/ARM with t_{avg} = 60 min, and (f) CERES/ARM with t_{avg} = 180 min. Black marker edges denote negative absorptance values.

cated and the slope of the best fit line is not a meaningful measure of cloud SW absorptance.

[51] Both RTMs produce almost perfectly linear relationships between TOA albedo and transmittance, as indicated by $RMSD_{l-q}$ values on the order of 10^{-3}. The slope $d\alpha_{TOA}/dT$ is approximately −0.9 in both cases. Because a surface albedo of 0.05 has been assumed, we expect the slope to have a magnitude of less than 0.95. (See the discussion following equation (5) in section 2.1.2.) Thus the cloud-induced absorption has reduced the slope by an additional 0.05.

[52] The physics in the radiative transfer models (conservation of energy, use of plane parallel clouds, etc.) force the transmittance and absorptance to be consistent, so that the absorptance cannot vary greatly. This can be seen in Figures 9a and 9b, as the model data points are nearly uniform in color. A closer look at the numerical data reveals that the model absorptance is actually slightly higher in the low transmittance range than in the high transmittance range. (The difference between the absorptance in these ranges is about 30% of the mean value for ARM RT and 18% for SARB.) This indicates that absorptance does indeed increase with cloud amount in the models, if only slightly.

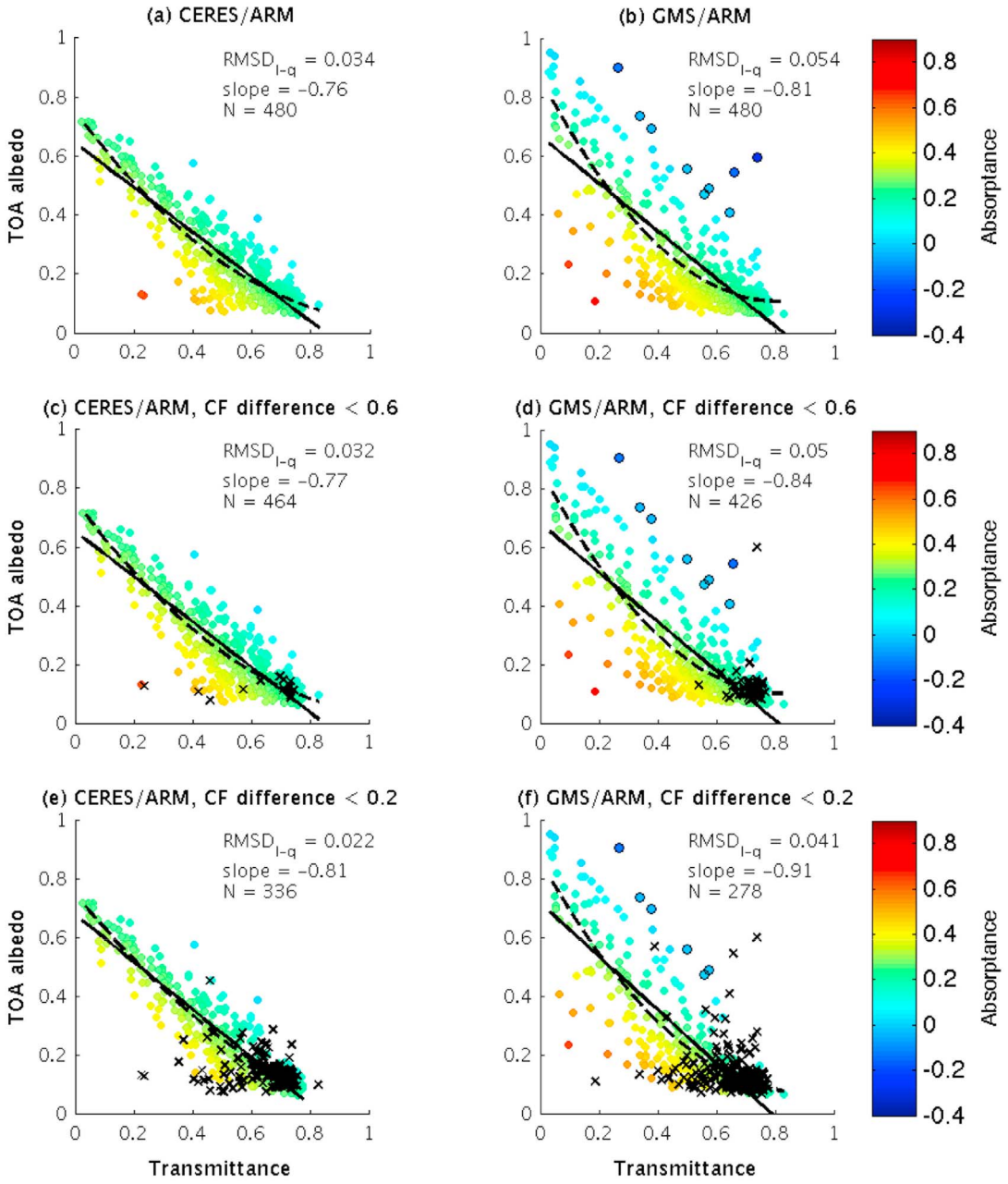

Figure 10. Plots of α_{TOA} versus T for (a, c, e) CERES/ARM and (b, d, f) GMS/ARM in which the difference between the satellite and surface measured cloud fraction (CF) is progressively restricted. No CF restriction (Figures 10a and 10b), $|\Delta CF| < 0.6$ (Figures 10c and 10d), and $|\Delta CF| < 0.2$ (Figures 10e and 10f). The averaging period for the surface data is 180 min. Black marker edges denote negative absorptance values, and crosses denote eliminated data.

[53] Although averaging intervals from 30 to 180 min were tested for the observational data sets, results for only t_{avg} = 60 and 180 min are used to illustrate the general results. In Figures 9c–9f, the points exhibit considerable scatter and the relationship between α_{TOA} and T is clearly nonlinear. Values of unexpectedly low transmittance in the low TOA albedo range combine to produce very high absorptance (yellow to red circles), pulling the quadratic fit down. There are also some values of high transmittance in the middle to high TOA albedo range, corresponding to low (blue circles) or even negative (open dots) absorptance. However, the linearity improves as the averaging time of the surface measurements is extended. For GMS/ARM, the $RMSD_{l-q}$ decreases from 0.061 to 0.055 as t_{avg} increases from 60 to 180 min. For CERES/ARM, the corresponding $RMSD_{l-q}$ values are 0.042 and 0.034. On the basis of this result, we conclude that at least some of the difference between model and observational absorption estimates does, in fact, stem from measurement mismatch. Since all of the $RMSD_{l-q}$ values for the observational data sets are more than 10× those computed

for the model data, we also conclude that 180 min is not a sufficient averaging time to remove sampling mismatch for these observations. As mentioned previously, a time restriction (09:00–15:00 LT) was applied to the observational data to avoid the complications associated with large SZAs. Because CERES observations of Manus from the Terra satellite are made in the morning (10:30–11:30 LT) and the surface averaging intervals are chosen to be centered on the satellite measurement time, testing longer averaging periods is not possible using these data.

[54] Although the best fit lines are not well defined for the observational data, it is clear that they are less steep than for the models. This indicates that apparent absorptance is increasing more quickly as transmittance declines for the measured data, which would lead to the observed model-measurement absorption bias. The best fit lines do steepen as the averaging time increases. For GMS/ARM, the slope goes from −0.64 to −0.81 when the averaging time is increased from 60 to 180 min; the corresponding values are −0.62 and −0.76 for CERES/ARM.

[55] The GMS TOA albedo has a more nonlinear distribution with respect to the measured transmittance (higher $RMSD_{l-q}$) than TOA albedo from CERES satellite measurements. Nevertheless, GMS/ARM also has a steeper best fit slope because of the high TOA albedo values, a clear illustration that the slope of the best fit line can be misleading when $d\alpha_{TOA}/dT$ is not linear. When a time average of GMS data is used instead of instantaneous values for the 3 h averages, the $RMSD_{l-q}$ (0.050) and the steepness of the slope (−0.79) are reduced (not shown), so this fit is likely more meaningful. The greater nonlinearity of $d\alpha_{TOA}/dT$ and the negative absorptance outliers indicate that the large standard deviation of GMS/ARM absorptance is likely a result of inaccuracy in the GMS TOA reflectances in addition to field of view mismatch between satellite and surface data.

5.2. Restricting the Satellite and Surface Observation Mismatch

[56] Besides averaging, another way to reduce field of view mismatch is to simply discard cases for which we know that the satellite and surface samples are not consistent. In this portion of the study, the difference between the time averaged cloud fraction observed from the surface (ARM) and the instantaneous spatial average of the cloud fraction within the satellite footprint (CERES or GMS) is used as a measure of spatial mismatch and data from occasions when this difference is large are excluded. Note that cloud fraction is not a complete measure of cloud field macroscopic properties; optical thickness and vertical extent are also important characteristics of clouds. However, cloud cover is the easiest cloud property to obtain from passive sensors and, to first order, has the greatest effect on the flow of radiation through the atmosphere. In addition, the fact that the cloud fraction distributions from the data sets analyzed here differ widely (as shown in Figure 5), suggests that this may be a fruitful approach.

[57] TOA albedo-transmittance plots in which the difference between the surface- and satellite-observed cloud fraction is progressively limited are displayed in Figure 10. Here the surface measurements have been averaged over 180 min intervals. As the CERES-ARM and GMS-ARM cloud fraction difference is reduced, the eliminated points are mostly in the low TOA albedo range. These include many cases of enhanced absorption in the mid transmittance range so that the $RMSD_{l-q}$ values decrease and the best fit lines become steeper. This again supports the theory that mismatch between the surface and TOA measurements causes enhanced values of observed absorptance. The CERES-ARM best fit slope progressively increases, but never reaches the magnitude of the slopes produced by the models (−0.81 versus about −0.90 for the models). When the GMS-ARM cloud fraction difference is limited to a maximum of 0.2, the GMS-ARM best fit line actually becomes slightly steeper than either model best fit line (−0.91). However, this precise value is not very meaningful since the relationship between the TOA and surface measurements is still rather nonlinear ($RMSD_{l-q}$ = 0.042). Excessively high (low) TOA albedo values are found even in the limited GMS data set for overcast (partly cloudy) conditions. The $RMSD_{l-q}$ is reduced to lower values for CERES/ARM than for GMS/ARM, which indicates that the mismatch between GMS and ARM is not reduced as efficiently or that the scatter in the GMS/ARM values obscures any improvements produced by the cloud fraction matching. In neither case does the $RMSD_{l-q}$ approach the small values (of order 10^{-3}) found for the model data.

5.3. Residual Nonlinearity

[58] Increasing the averaging time for the surface measurements to 180 min and limiting the difference between TOA and surface observed cloud fraction to 0.2 or less, even in combination, cannot completely eliminate the nonlinearity in the α_{TOA} versus T plots for the combined surface-satellite data sets at Manus. The most plausible explanations are that either there is still some difference between the TOA and surface measurements, such as cloud optical depth or apparent geometry, that has not been removed or that the nonlinearity is not an artifact but the result of three-dimensional (3-D) radiative transfer effects. *Cess et al.* [1996] mention that enhancement of the surface downwelling flux by scattering from the sides of nearby clouds could cause nonlinearity similar to that produced by TOA-surface mismatch. *O'Hirok and Gautier* [1998] simulated 3-D radiative transport through a tropical scene containing strongly convective clouds, finding that the absorption could be on the order of 12 W m^{-2} higher than that obtained using a model that accounted for horizontal variability of atmospheric and cloud properties but not horizontal fluxes. *Barker and Li* [1997] criticized the α_{TOA} versus T method and used a 3-D Monte Carlo RTM to demonstrate that horizontal fluxes can reduce the slope of the best fit line, leading to false conclusions of anomalous absorption. They also found that the relatively smaller field of view of surface pyranometers compared to satellite-based radiometers adds to the nonlinearity and reduces the slope further.

[59] Although 3-D effects tend to average out over time if the scene evolves through either cloud dynamical processes or simple advection, they nearly always increase the observed absorption. This would lead to a negative model-measurement absorption bias in our results, since two-stream models do not include horizontal transport. If, indeed, some of the difference between model and measured absorption in cloudy columns is attributable to 3-D effects,

this portion of the difference would be due to inadequacies of the radiative transfer models rather than the observations.

[60] Three-dimensional effects are generally greater for lower solar elevation angles, so restricting our consideration to times between 09:00 and 15:00 LT tends to minimize 3-D effects. Nevertheless, the plots in Figure 9 support the 3-D effect argument to some degree. Three-dimensional effects are known to increase with cloud field inhomogeneity. In Figure 9, points with large values of absorptance that appear to contribute to the nonlinearity of the observational data are primarily found in the middle to high transmittance, low TOA albedo range. Assuming that transmittance is a rough measure of cloud cover, these values correspond to cases of broken or scattered clouds. No corresponding high absorptance values are observed in this range for the RTMs. Thus, the models and observations do not agree well for broken cloudy conditions, leading to many cases of negative model-measurement absorption differences that may be due to the effect of 3-D radiative transfer on the observations.

6. Summary and Conclusions

[61] Values of SW absorption calculated from collocated instantaneous satellite measurements and time-averaged surface measurements are compared to corresponding values obtained from radiative transfer (RT) models. The observational data sets used are surface broadband SW measurements from the ARM research facility at Manus Island, and collocated TOA observations from the geostationary GMS-5 satellite and CERES. The RTMs, referred to as ARM RT and SARB, are both based on the Fu-Liou radiative transfer numerical code, but differ in that they have surface and TOA measurements as input, respectively. Model B, which is a simpler model with CERES data as input, is not included in the analysis because the Model B surface SW fluxes are similar to the SARB fluxes. The observational and model estimates of TOA and surface SW fluxes are found to be generally highly correlated, though the ARM RT fluxes are somewhat different than the others.

[62] Modeled and observed column SW absorption show low correlation and statistically significant mean differences. The model-observation absorption bias is found to be negative (observed absorption > model absorption) with a magnitude of between 13 and 32 W m^{-2}, depending on details of the analysis. Relatively small differences in TOA and surface SW fluxes can add up to significant absorption discrepancies. Though the ARM RT and SARB fluxes are not strongly correlated, both models produce surface and TOA SW fluxes that closely mirror each other, so that the absorption values are always within a narrow range. Instantaneous satellite observations and time-averaged surface observations of TOA and surface SW fluxes often fail to mirror each other, resulting in very high or low, even negative, values of absorption.

[63] Plots of TOA albedo versus transmittance show that α_{TOA} and T determined from the observations are not linearly related. This is likely a result of field of view mismatch between the satellite and surface SW flux measurements. The slope of the best fit line is used as a measure of cloud absorption and the RMSD between linear and quadratic fits as an estimate of departure from linearity. When the averaging time of the surface data was increased, the $RMSD_{l\text{-}q}$ declined and the best fit line became steeper. When occasions of large cloud fraction differences were also excluded, the $RMSD_{l\text{-}q}$ again decreased and the best fit line steepened. These results imply that sampling issues contribute to the observed nonlinearity and excess absorption compared to model predictions. Averaging surface data over one or a few hours does not seem to be enough to eliminate the mismatch. Since the measures of absorption used in this study (column SW absorption and the slope of α_{TOA} versus T) are sensitive to mismatches between TOA and surface SW fluxes, cloud SW absorption cannot be assessed with high confidence even using some of the best available observational data sets.

[64] The observations still produce lower slopes than the models even after using a long (3 h) averaging time for the surface data and discarding samples for which satellite and surface cloud fractions disagree. This is most likely due to 3-D transport through cloudy or remaining field of view mismatch. (Even when cloud fractions are the same, the satellite and surface instruments may observe clouds of different height and optical thickness.) However, the existence of some absorption not accurately portrayed by the models cannot be completely ruled out. No other explanation is immediately obvious.

[65] The ergodic assumption in meteorological applications has not (to the authors' knowledge) been closely examined for tropical conditions. An averaging time of 60 min for surface data was judged sufficient by *Cess et al.* [1996]; however, this was determined for radiation data from Wisconsin. It is not obvious that the same would be true at Manus. Weather conditions and the time and spatial scale of cloud formation processes are different at a tropical island than at a midlatitude site like Wisconsin. In order for the instantaneous spatial average within the satellite grid box to be replaceable by a time average of surface data, the sampled cloud distribution must be statistically stationary over the corresponding spatial and temporal scales. Thus the ergodic assumption may not hold under all meteorological or measurement conditions. This issue requires further investigation.

Notation

α_{sfc}	surface albedo.
α_{TOA}	TOA albedo.
τ_{aer}	aerosol optical depth.
τ_{ice}	optical depth of ice crystals in a cloud.
τ_{liq}	optical depth of liquid water in a cloud.
A	column SW absorptance.
F_A	SW flux absorbed in the atmosphere.
$F\uparrow_{TOA}$	upwelling SW flux at the TOA.
$F\downarrow_{TOA}$	downwelling SW flux at the TOA.
$F\uparrow_{sfc}$	upwelling SW flux at the surface.
$F\uparrow_{TOA}$	downwelling SW flux at the surface.
R	Pearson correlation coefficient.
t_{avg}	averaging time of the surface data (ARM).
T	atmospheric transmittance.

[66] **Acknowledgments.** We are grateful to Mandy Khaiyer and David Rutan of Science Systems and Applications, Inc., for spending considerable time answering questions about the GMS and SARB data sets. We thank Chuck Long of the Pacific Northwest National Laboratory for providing the processed surface measurement data. GMS data at Manus

were obtained from the Atmospheric Radiation Measurement Program of the U.S. Department of Energy. The surface flux data supplied by Chuck Long were also based on Atmospheric Radiation Measurement Program measurements. CERES data were supplied by the NASA Langley Research Center Atmospheric Science Data Center. Support for this research was provided by the Department of Energy Atmospheric Research Program, DOE grant DE-SC0001635, and by NASA grant NNX08AT46G, through the NASA/GEWEX Surface Radiation Budget project.

References

Ackerman, T. P., D. M. Flynn, and R. T. Marchland (2003), Quantifying the magnitude of anomalous solar absorption, *J. Geophys. Res.*, *108*(D9), 4273, doi:10.1029/2002JD002674.

Asano, S., A. Uchiyama, Y. Mano, M. Murakami, and Y. Takayama (2000), No evidence for solar absorption anomaly by marine water clouds through collocated aircraft measurements, *J. Geophys. Res.*, *105*, 14,761–14,775.

Barker, H. W., and Z. Li (1997), Interpreting shortwave albedo-transmittance plot: True or apparent anomalous absorption?, *Geophys. Res. Lett.*, *24*, 2023–2026.

Bloom, S., et al. (2005), Documentation and validation of the Goddard Earth Observing System (GEOS) Data Assimilation System, version 4, *Tech. Rep. Ser. Global Model. Data Assimilation 104606*, NASA Goddard Space Flight Cent., Greenbelt, Md.

Byrne, R. N., R. C. J Somerville, and B. Murakami (1996), Broken-cloud enhancement of solar radiation absorption, *J. Atmos. Sci.*, *53*, 878–886.

Cess, R. D., et al. (1995), Absorption of solar radiation by clouds: Observations versus models, *Science*, *267*, 469–499.

Cess, R. D., M. H. Zhang, Y. Zhou, X. Jing, and V. Dvortsov (1996), Absorption of solar radiation by clouds: Interpretations of satellite, surface and aircraft measurements, *J. Geophys. Res.*, *101*, 23,299–23,309.

Chiu, J.-Y. C., A. Marshak, and W. J. Wiscombe (2004), The effect of surface heterogeneity on cloud absorption estimates, *Geophys. Res. Lett.*, *31*, L15105, doi:10.1029/2004GL020104.

Clarke, A. D., and V. N. Kapustin (2002), A Pacific aerosol survey. Part I: A decade of data on particle production, transport, evolution, and mixing in the troposphere, *J. Atmos. Sci*, *59*, 363–382.

Conant, W. C., A. M. Vogelmann, and V. Ramanathan (1998), The unexplained solar absorption and atmospheric H_2O: A direct test using clear-sky data, *Tellus, Ser. B*, *50*, 526–534.

Francis, P. N., J. P. Taylor, P. Hignett, and A. Slingo (1997), On the question of enhanced absorption of solar radiation by clouds, *Q. J. R. Meteorol. Soc.*, *123*, 419–434.

Fu, Q., and K. N. Liou (1992), On the correlated k-distribution method for radiative transfer in nonhomogeneous atmospheres, *J. Atmos. Sci.*, *49*, 2139–2156.

Gupta, S. K., D. P. Kratz, P. W. Stackhouse, and A. C. Wilber (2001), The Langley Parameterized Shortwave Algorithm (LPSA) for surface radiation budget studies, version 1.0, *Rep. NASA/TP-2001-211272*, NASA, Washington, D. C.

Imre, D. G., E. H. Abramson, and P. H. Daum (1996), Quantifying cloud-induced shortwave absorption: An examination of uncertainties and of recent arguments for large excess absorption, *J. Appl. Meteorol.*, *35*, 1991–2010.

Kisho Eisei Senta (1997), *The GMS User*'s *Guide*, 3rd ed., Meteorol. Satell. Cent., Jpn. Meteorol. Agency, Tokyo.

Kratz, D. P., S. K. Gupta, A. C. Wilber, and V. E. Sothcott (2010), Validation of the CERES edition 2B surface-only flux algorithms, *J. Appl. Meteorol. Climatol.*, *49*, 164–180, doi:10.1175/2009JAMC2246.1.

Li, Z., A. P. Trishchenko, H. W. Barker, G. L. Stephens, and P. Partain (1999), Analyses of Atmospheric Radiation Measurement (ARM) program's enhanced shortwave experiment (ARESE) multiple data sets for studying cloud absorption, *J. Geophys. Res.*, *104*, 19 127–19 134.

Loeb, N. G., S. Kato, K. Loukachine, N. Manalo-Smith, and D. R. Doelling (2007), Angular distribution models for top-of-atmosphere radiative flux estimation from the clouds and the Earth's radiant energy system instrument on the terra satellite. Part II: Validation, *J. Atmos. Oceanic Technol.*, *24*, 564–583.

Long, C. N., and T. P. Ackerman (1995), Surface measurements of solar irradiance: A study of the spatial correlation between simultaneous measurements at separated sites, *J. Appl. Meteorol.*, *34*, 1039–1046.

Long, C. N., T. P. Ackerman, K. L. Gaustad, and J. N. S. Cole (2006), Estimation of fractional sky cover from broadband shortwave radiometer measurements, *J. Geophys. Res.*, *111*, D11204, doi:10.1029/2005JD006475.

Lubin, D., J.-P. Chen, P. Pilewskie, V. Ramanathan, and F. P. J. Valero (1996), Microphysical examination of excess cloud absorption in the tropical atmosphere, *J. Geophys. Res.*, *101*, 16,961–16,972.

Mather, J. H. (2005), Seasonal variability in clouds and radiation at the Manus ARM site, *J. Clim.*, *18*, 2417–2428.

Mather, J. H., T. P. Ackerman, and M. P. Jensen (1998), Characteristics of the atmospheric state and the surface radiation budget at the tropical western Pacific ARM site, *Geophys. Res. Lett.*, *25*, 4513–4516.

Mather, J. H., S. A. McFarlane, M. A. Miller, and K. L. Johnson (2007), Cloud properties and associated radiative heating rates in the tropical western Pacific, *J. Geophys. Res.*, *112*, D05201, doi:10.1029/2006JD007555.

McFarlane, S. A., J. H. Mather, T. P. Ackerman, and Z. Liu (2008), Effect of clouds on the calculated vertical distribution of shortwave absorption in the tropics, *J. Geophys. Res.*, *113*, D18203, doi:10.1029/2008JD009791.

Melnikova, I. N., and A. V. Vasilyev (2005), *Short-Wave Solar Radiation in the Earth*'s *Atmosphere: Calculation, Observation and Interpretation*, chap. 3, pp. 115–121, Springer, Berlin.

Minnis, P., P. W. Heck, and D. F. Young (1993), Inference of cirrus cloud properties using satellite-observed visible and infrared radiances. Part II: Verification of theoretical cirrus radiative properties, *J. Atmos. Sci.*, *50*, 1305–1321.

Minnis, P., W. L. Smith Jr., D. Garber, K. Ayers, and D. R. Doelling (1995), Cloud properties derived from GOES-7 for the spring 1994 ARM intensive observing period using version 1.0.0 of ARM satellite data analysis program, *Rep. NASA-RP-1366*, NASA, Washington, D. C.

O'Hirok, W., and C. Gautier (1998), A three-dimensional radiative transfer model to investigate the solar radiation within a cloudy atmosphere. Part I: Spatial effects, *J. Atmos. Sci.*, *55*, 2162–2179.

Payne, R. E. (1972), Albedo of the sea surface, *J. Atmos. Sci.*, *29*, 959–970.

Peixoto, J. P., and A. H. Oort (1992), *Physics of Climate*, pp. 12–13, Springer, New York.

Pilewskie, P., and F. P. J. Valero (1995), Direct observations of excess solar absorption by clouds, *Science*, *267*, 1626–1629.

Ramanathan, V., B. Subaşilar, G. Zhang, W. Conant, R. Cess, J. Kiehl, H. Grassl, and L. Shi (1995), Warm pool heat budget and shortwave cloud forcing: A missing physics?, *Science*, *267*, 499–503.

Ramaswamy, V., and S. M. Freidenreich (1998), A high-spectral resolution study of the near-infrared solar flux disposition in clear and overcast atmospheres, *J. Geophys. Res.*, *103*, 23,255-23,273.

Rutan, D., F. Rose, M. Roman, N. Manalo-Smith, C. Schaaf, and T. Charlock (2009), Development and assessment of broadband surface albedo from Clouds and the Earth's Radiant Energy System Clouds and Radiation Swath data product, *J. Geophys. Res.*, *104*, D08125, doi:10.1029/2008JD010669.

Sasheeth, S. K., and K. Krishna Moorthy (2005), Radiative effects of natural aerosols: A review, *Atmos. Environ.*, *39*(11), 2089–2110.

Sengupta, M., and T. P. Ackerman (2003), Investigating anomalous absorption using surface measurements, *J. Geophys. Res.*, *108*(D24), 4761, doi:10.1029/2003JD003411.

Smirnov, A., B. N. Holben, Y. J. Kaufman, O. Dubovik, T. F. Eck, I. Slutsker, C. Pietras, and R. N. Halthore (2002), Optical properties of atmospheric aerosol in maritime environments, *J. Atmos. Sci.*, *59*(3), 501–523.

Stephens, G. L., and S.-C. Tsay (1990), On the cloud absorption anomaly, *Q. J. R. Meteorol. Soc.*, *116*, 671–704.

Stephens, G. L., and P. J. Webster (1979), Sensitivity of radiative forcing to variable cloud and moisture, *J. Atmos. Sci.*, *36*, 1542–1556.

Stoffel, T. (2004), GNDRAD handbook, *Rep. ARM TR-027*, U.S. Dep. of Energy, Washington, D. C.

Troyan, D. (2010), Merged sounding value-added product, *DOE/SC-ARM/TR-087*, Dep. of Energy, Washington, D. C.

Wielicki, B. A., et al. (1998), Clouds and the Earth's Radiant Energy System (CERES): Algorithm overview, *IEEE Trans. Geosci. Remote Sens.*, *36*, 1127–1139.

T. P. Ackerman and L. M. Hinkelman, Joint Institute for the Study of the Atmosphere and Ocean, University of Washington, PO Box 355672, Seattle, WA 98195-5672, USA.

S. A. McFarlane, Climate Physics Group, Pacific Northwest National Laboratory, PO Box 999, MS K9-24, Richland, WA 99352, USA.

K. Parding, Geophysical Institute, University of Bergen, Postboks 7803, N-5007 Bergen, Norway. (kajsa.parding@gfi.uib.no)